Available online at www.sciencedirect.com

SciVerse ScienceDirect

Ceramics International 38 (2012) 4253–4261

CERAMICS INTERNATIONAL

www.elsevier.com/locate/ceramint

Synthesis, structural and electrical properties of novel pyrochlores in the Bi_2O_3–CuO–Ta_2O_5 ternary system

M.P. Chon [a], K.B. Tan [a,*], C.C. Khaw [b], Z. Zainal [a], Y.H. Taufiq-Yap [a], P.Y. Tan [a]

[a] Department of Chemistry, Faculty of Science, Universiti Putra Malaysia, 43400 Serdang, Selangor, Malaysia

[b] Department of Mechanical and Material Engineering, Faculty of Engineering and Science, Universiti Tunku Abdul Rahman, 53300 Setapak, Kuala Lumpur, Malaysia

Received 20 December 2011; received in revised form 31 January 2012; accepted 1 February 2012
Available online 9 February 2012

Abstract

A series of non-stoichiometric cubic pyrochlores with general formula, $Bi_{3-x}Cu_{1.8}Ta_{3+x}O_{13.8+x}$ (BCT) was successfully prepared by solid state reaction at the firing temperature of 950 °C over 2 days. The solid solution mechanism is proposed as one-to-one replacement of Bi^{3+} for Ta^{5+}, together with a variation in oxygen content in order to achieve electroneutrality. The solid solution limit is confirmed by X-ray diffraction technique (XRD) for which linear variation of lattice constants is observed at $0 \leq x \leq 0.6$. The refined lattice constants are found to be in the range of 10.4838 (8) Å–10.5184 (4) Å and the grain sizes of these samples determined by scanning electron microscopy (SEM) fall between 1 and 40 μm. Meanwhile, thermal analyses show no physical or chemical change for the prepared pyrochlores. The relative densities of the densified pellets for AC impedance measurements are above 85% and the measured relative permittivity, ε' and dielectric loss, tan δ for composition, $x = 0.2$ at ambient temperature are ~60 and 0.07 at 1 MHz, respectively. The calculated activation energies are 0.32–0.40 eV and the conductivity values, Y' are in the order of 10^{-3} at 400 °C. The conduction mechanisms of BCT pyrochlores are probably attributed to the oxygen non-stoichiometry and mixed valency of copper within the structure.

Keywords: A. Powders: solid state reaction; B. X-ray methods; C. Electrical properties; D. Tantalates

1. Introduction

Careful studies have been performed on pyrochlore oxides which have wide variety of chemical compositions, extraordinary structural behaviors and electrical properties [1–5]. Recent investigations on Bi-based pyrochlores have revealed interesting correlation between dielectric properties and structure of these materials [2,6–8]. In general, Bi_2O_3-based materials are unique because of their low firing and sintering temperature, e.g. 800–950 °C, unreactive behavior towards electrodes, allowing them to be co-fired with Ag for the preparation of multilayer devices with wide range of permittivities [9,10]. Pyrochlore oxides exhibit excellent exploitable properties due to their ability to form substituted and defective structures in which compositions and properties could be tailored made by means of doping. Hence, pyrochlore oxides often demonstrate outstanding electrical properties which include dielectric, ferroelectric, piezoelectric, ionic conductivity and temperature – stable permittivity properties [11,12].

The pyrochlore oxides of general formula $A_2B_2O_7$ have cubic crystal structure with eight formula units per unit cell and lattice constant of around 10 Å. The larger cation at A site is coordinated to eight oxygen atoms and a smaller B cation is six-fold coordinated element [11]. It is often written as $A_2B_2O_6O'$ to distinguish the oxygen atoms in two different networks, A_2O' and B_2O_6. The A_2O' attributes that the structure is built of two interpenetrating networks with four-coordinate O′ ions and two-coordinate A cations. The B_2O_6 framework exists as [BO_6] octahedra that share all vertices to form a three dimensional network based on a diamond net. This results in large cavities containing the O′ and A atoms in cuprite-like A_2O tetrahedral net [13].

Bismuth-based pyrochlores of general formula $Bi_{3/2}M^{2+}X_{3/2}O_7$ (M = Zn, X = Nb, Ta, Sb) stoichiometry can be expressed as $(Bi_{3/2}M_{1/2})(M_{1/2}X_{3/2})O_7$ in which the M^{2+} ion occupies both

* Corresponding author. Tel.: +60 3 8946 7491; fax: +60 3 8943 5380.
E-mail address: tankb@science.upm.edu.my (K.B. Tan).

0272-8842/$36.00
doi:10.1016/j.ceramint.2012.02.007

A- and B-sites [14–16]. As analogous to the reported Bi_2O_3–ZnO–Nb_2O_5 (BZN) system, there are two major structural variations in Bi_2O_3–ZnO–Ta_2O_5 (BZT) system: (i) a cubic pyrochlore, $(Bi_{3/2}Zn_{1/2})(Zn_{1/2}Ta_{3/2})O_7$ (α-BZT) and (ii) a lower symmetry zirconolite phase, $Bi_2(Zn_{1/3}Ta_{2/3})_2O_7$ (β-BZT). In BZT system, both compositions were studied as potential candidates for microwave dielectrics [17]. The reported α-BZT has permittivity and dielectric loss of 58 and 0.0023 at 30 °C, respectively and temperature coefficient of capacitance (TCC) of −156 ppm/°C in the range of 30 °C −300 °C at 1 MHz [18]. In our present study, Cu^{2+} is chosen to replace Zn^{2+} mainly attributed to close similarity in ionic radii of these divalent transition metal cations. To date, there appears limited literature and study in the Bi_2O_3–CuO–Ta_2O_5 (BCT) ternary system notably, their composition–structure–property correlation remains unclear. Hence, we commenced a detailed study to understand the fundamentals of BCT pyrochlores in view of the excellent dielectric properties which found in α-BZT analogue. The preparation of novel $Bi_{3-x}Cu_{1.8}Ta_{3+x}O_{13.8+x}$ pyrochlore subsolidus solution and their structural and electrical properties are reported in this paper.

2. Experimental

Pyrochlore samples with the proposed formula $Bi_{3-x}Cu_{1.8}$-$Cu_{1.8}Ta_{3+x}O_{13.8+x}$ where $-0.2 \leq x \leq 0.8$ were prepared by solid state technique. The stoichiometric amounts of high purity oxides, Bi_2O_3 (99.9%, Acros Organics), CuO (99.7%, Alfa Aesar) and Ta_2O_5 (99.85%, Alfa Aesar) were used as starting materials and mixed with sufficient acetone in an agate mortar before firing at 950 °C for two days. At the initial stage, the mixture was pre-fired at 300 °C and 600 °C, respectively for 2 h and 800 °C overnight in order to avoid significant bismuth weight loss. The phase purity of the prepared samples was confirmed by X-ray diffraction (XRD) analysis using an automated Shimazu CuKα radiation X-ray diffractometer. XRD data were collected for routine scan at 2.0° step size whereas 0.1° was used for lattice refinement using Chekcell program. The phase pure samples were compacted into pellets with average thickness of 1.40 mm, diameter of 7.38 mm and sintered at 950 °C.

The densified pellets were coated with platinum paste prior to electrical measurement by an AC impedance analyser, Hewlett Packard LF HP4192A in the frequency range of 5 Hz to 13 MHz. Different regions of the materials were characterised according to their electrical relaxation times or time constants. The analysis was performed at the temperature range of approximately 27–800 °C on both heating and cooling cycles, with every 50 °C interval. The electrical data were collected after 15 min of thermal equilibrium. Meanwhile, thermal analyses were carried out by differential thermal analysis (Perkin Elmer DTA7) and thermogravimetric (Perkin Elmer TGA), respectively. The surface morphologies of the densified pellets were examined using scanning electron microscopy, LEO 1455 VPSEM and the absorption bands of pyrochlore materials were determined by Fourier transform infrared spectroscopy (Perkin Elmer, 100 series FTIR).

3. Results and discussion

3.1. Phase formation and solid solution mechanism

From the results of heating for various durations and at temperatures in the range of 950–1000 °C, it is found that the $Bi_{3-x}Cu_{1.8}Ta_{3+x}O_{13.8+x}$ pyrochlore samples are fully formed after heating for 2 days at 950 °C. Fig. 1 shows the XRD patterns of the non-stoichiometric $Bi_{3-x}Cu_{1.8}Ta_{3+x}O_{13.8+x}$ samples crystallised in cubic structure. The diffraction peaks could be fully indexed based on space group *Fd3m*, No. 277 similar to that of α-BZT analogue. At 950 °C, sample with the highest Bi content, i.e. $x = -0.20$ contains cubic, $BiTaO_4$ and monoclinic zirconolite phases while, at $x = 0.80$, secondary phase $CuTa_2O_6$ is discernable as shown in inset Fig. 1. The refined lattice constants are found to be in the range of 10.4838 (8) Å–10.5184 (4) Å. It is believed that the larger ionic radius of Bi^{3+} (1.17 Å) has contributed to the increased lattice constants [1] and hence, by the removal of Bi content, a linear decrease of lattice constants in BCT samples is observed (Fig. 2). Such characteristic fulfills the Vegard's law and subsolidus solution limit is therefore confirmed as $0 \leq x \leq 0.60$. The formation mechanism is proposed as one-to-one replacement of Bi^{3+} for Ta^{5+} together with a variation of oxygen concentration within the subsolidus solution. Substitution of higher valence cation, Ta^{5+} by lower valence cation, Bi^{3+} is likely to have been compensated by creating interstitial oxygen or vacancies in order to maintain the charge neutrality. Meanwhile, at lower bismuth content, formation of high symmetry cubic phase is encouraged as the coupling effect of Bi $6s^2$ lone pair electrons is reduced [19]. The study of correlation between monoclinic zirconolite and cubic pyrochlore in BCT system is currently in progress. Different phase assemblages and compatibilities have been identified in our unpublished phase diagram results.

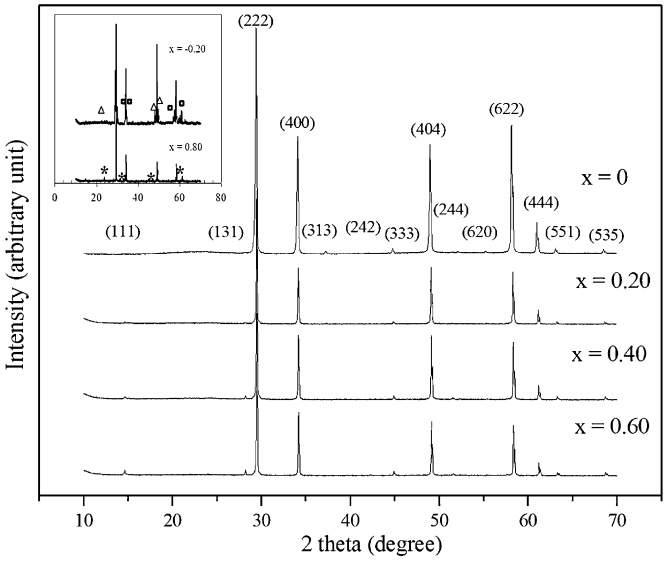

Fig. 1. XRD patterns of the prepared $Bi_{3-x}Cu_{1.8}Ta_{3+x}O_{13.8+x}$ samples, $-0.20 \leq x \leq 0.80$. $BiTaO_4$ (Δ); monoclinic zirconolite (□) and $CuTa_2O_6$ (*).

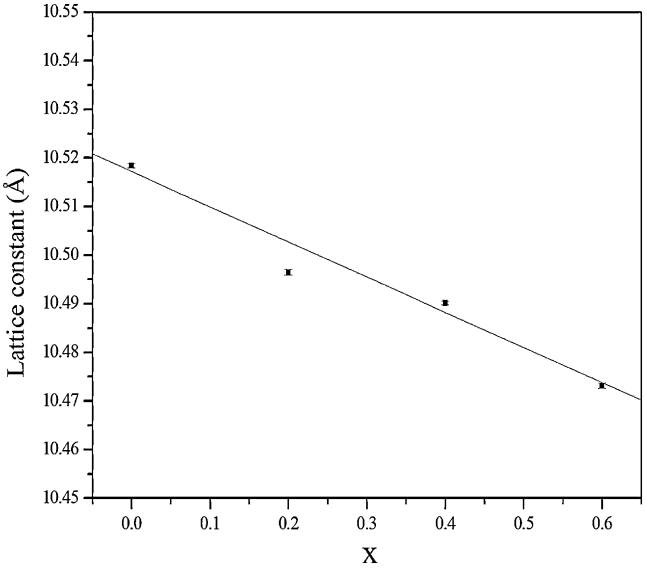

Fig. 2. Lattice constants as a function of x in the series of $Bi_{3-x}Cu_{1.8}Cu_{1.8}Ta_{3+x}O_{13.8+x}$.

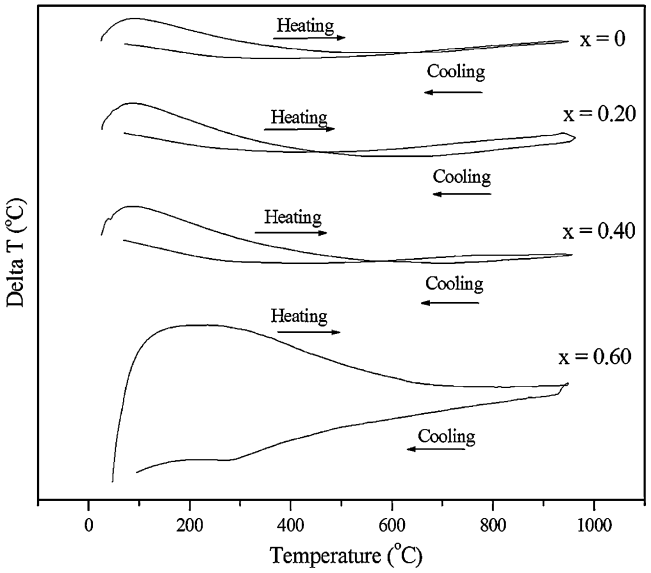

Fig. 4. DTA thermograms of $Bi_{3-x}Cu_{1.8}Ta_{3+x}O_{13.8+x}$ series.

On the other hand, weight-loss studies indicate that Bi_2O_3 volatilization is not a problem for all the samples and they are thermally stable, i.e. no thermal change, phase transition or loss of weight throughout the studied temperatures range. This is confirmed by TGA/DTA thermal analyses as shown in Figs. 3 and 4.

There are few important aspects to be considered concerning the stability of pyrochlore, e.g. cations electronegativity, ionic radii, charge neutrality and thermodynamic stability of phases [11]. At the outset, oxidation states of cations in BCT pyrochlores are assumed to be Bi^{3+}, Cu^{2+} and Ta^{5+}, respectively. The distribution of copper ions is interesting and might not be same as the analogues in the Bi_2O_3–ZnO–X_2O_5 (X = Nb, Ta) ternary systems as the reported highest coordination for Cu^{2+} is only 6 with ionic radius of 0.73 Å [20]. Structural distortion or deformation could be anticipated if copper ions enter the eight-fold coordinated A-sites. However, again, there is considerable uncertainty since there is strong and self-compensating correlation between variable compositions, atomic coordinates, occupancy and size of ionic radii which make it extremely difficult to deduce the pyrochlore structure of BCT system. As mentioned earlier, if A-sites are fully occupied by Bi ions, the coupling among $6s^2$ lone pairs might cause cell distortion, leading to the formation of orthorhombic phase [19]. The coupling among Bi ions could be broken if considerable amount of copper ions entering A-sites. Hence, a compromise is expected to the extent of compositional variables and distribution of copper ions over both sites and/or maybe involving off-center displacement of A cations to the higher multiplicity sites, e.g. *32e* or *96g* positions [13,21,22]. Ideally, the pyrochlores are almost never meant to be ordered and perfect in structure. Irregular BO_6 octahedra are common and variation of x parameter values of O(1) may result in perfect or distorted BO_6 octahedra and AO_8 cube, respectively. It is noteworthy that the tolerance factor has been introduced in the perovskites or structurally related aurivillius phases, but until recently, similar method has been revised in the pyrochlore systems [23–25]. Such approach should provide good indication to determine the structural stability and electrical properties of this complex family of pyrochlore oxides.

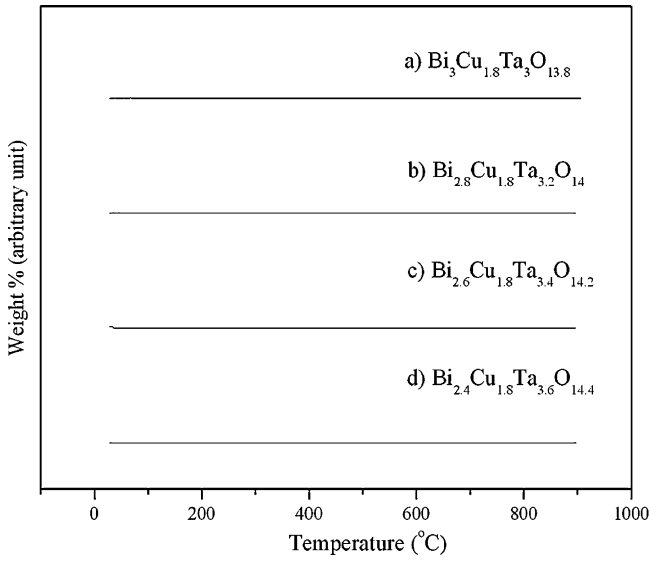

Fig. 3. TGA thermograms of $Bi_{3-x}Cu_{1.8}Ta_{3+x}O_{13.8+x}$ series.

The crystallite sizes of pyrochlores are estimated by the Williamson–Hall and Scherrer methods and these values are highly inter-correlated. Based on the Scherrer method, crystallite size (T) is calculated based on the formula:

$$T = 0.9 \times \frac{\lambda}{\beta \cos\theta} \quad (1)$$

and for the W–H method, the strain-induced broadening and crystallite size are deduced by:

$$\beta \cos\theta = \frac{k\lambda}{D} + 4\varepsilon \sin\theta \quad (2)$$

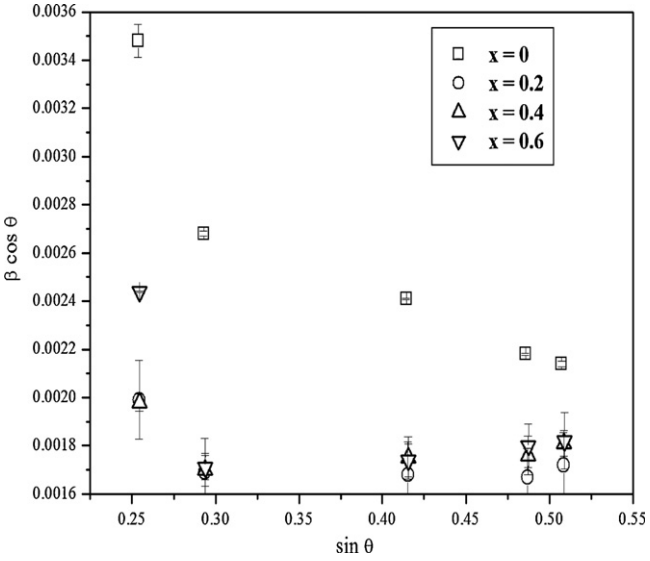

Fig. 5. Williamson–Hall plot with five intense X-ray diffraction peaks.

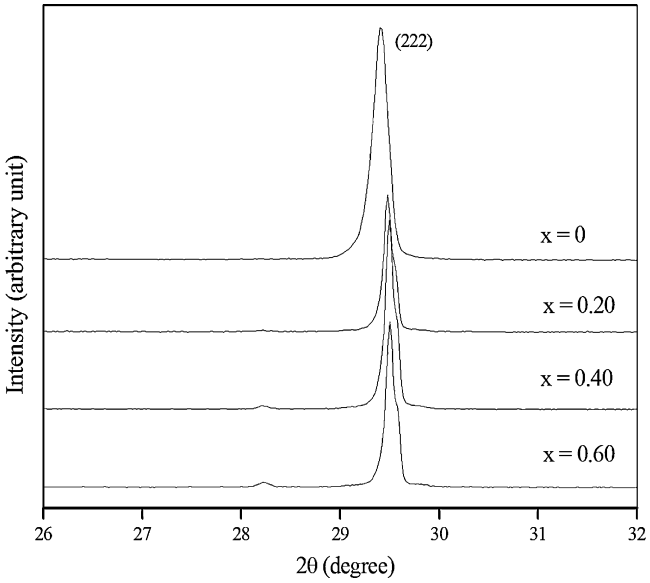

Fig. 6. Constant shift of (2 2 2) diffraction plane for $0 \leq x \leq 0.60$.

where β is the full width at half maximum (FWHM, in rad); θ is the scattering angle; λ = 1.5418 Å; k is the shape factor, 0.9; D is the coherent scattering length (crystallite size) and ε is the internal strain. For quantitative comparison, the five intense diffraction planes are chosen in the line broadening analysis (Fig. 5) and the integral breadth, β, crystallite size and internal strain for each sample are presented in Table 1. It is recognised that the degree of lattice strain in the samples strongly depends on coordination environment or amount of substitution in the case of doped samples, which may lead on to crystal imperfections [26]. The higher ε values, determined from the gradients for both end members, i.e. $x = 0$ and 0.6 indicate that the solid solution limit is achieved (Fig. 5 and Table 1). Meanwhile, X-ray broadening is used for the study of dislocation distribution and the peak broadening caused by lattice strain arising from lattice imperfection [27]. This is evidently shown in which sample, $x = 0$ has the highest ε and the broadest (2 2 2) diffraction plane. The peak position of (2 2 2) plane shows a constant shift of 2θ value towards a slightly higher angle for sample with lower bismuth content (Fig. 6). It should be noted that the peak broadening is also influenced by simultaneous small particle size and strain broadening (Fig. 7). Crystallite size and lattice strain could affect the Bragg peak in several ways and both have contributed to line peak width, intensity of the peak and shift of 2θ peak position, accordingly [28,29].

Table 1
Geometrical parameters of the prepared $Bi_{3-x}Cu_{1.8}Ta_{3+x}O_{13.8+x}$ pyrochlores.

x	d_{222} spacing (Å)	Lattice constants (Å)	Scherrer method (nm)	W–H method (nm)	W–H plot strain, ε
0	3.0372	10.5184 (4)	40	32	0.0011
0.2	3.0283	10.4965 (5)	72	63	0.0004
0.4	3.0272	10.4880 (4)	72	66	0.0003
0.6	3.0264	10.4838 (8)	59	53	0.0006

3.2. Microstructural analysis

Micrographs of $Bi_{3-x}Cu_{1.8}Ta_{3+x}O_{13.8+x}$ samples sintered at 950 °C are shown in Fig. 8. The samples densities are calculated geometrically and the values are found to be greater than 85% of theoretical densities for pellets sintered at 950 °C for 2 days. It is found that prolonged sintering has contributed towards higher relative density. The determined grain sizes of the pyrochlore samples are in the range of 1–40 μm. In general, composition with $x = 0$ displays large, well-defined and closely packed grains (Fig. 8a). Smaller crystallites in the order of 10^{-9} m (Section 3.1) imply that these grains consisted of several crystallites. Meanwhile, sample at $x = 0.2$ (Fig. 8b) shows much smaller grains together with several pores on the surface and the porosity increases from composition $x = 0$ to $x = 0.6$. The decrease in grain sizes with increasing x values in

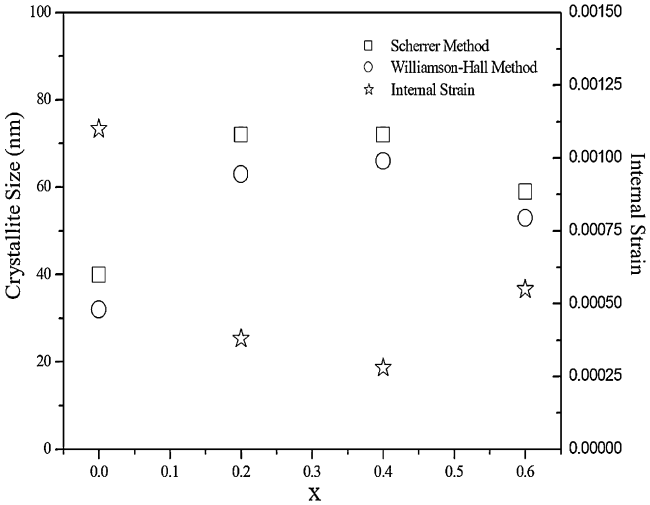

Fig. 7. Comparison between crystallite size calculated by two methods and the internal strain for each composition is plotted as a function of x.

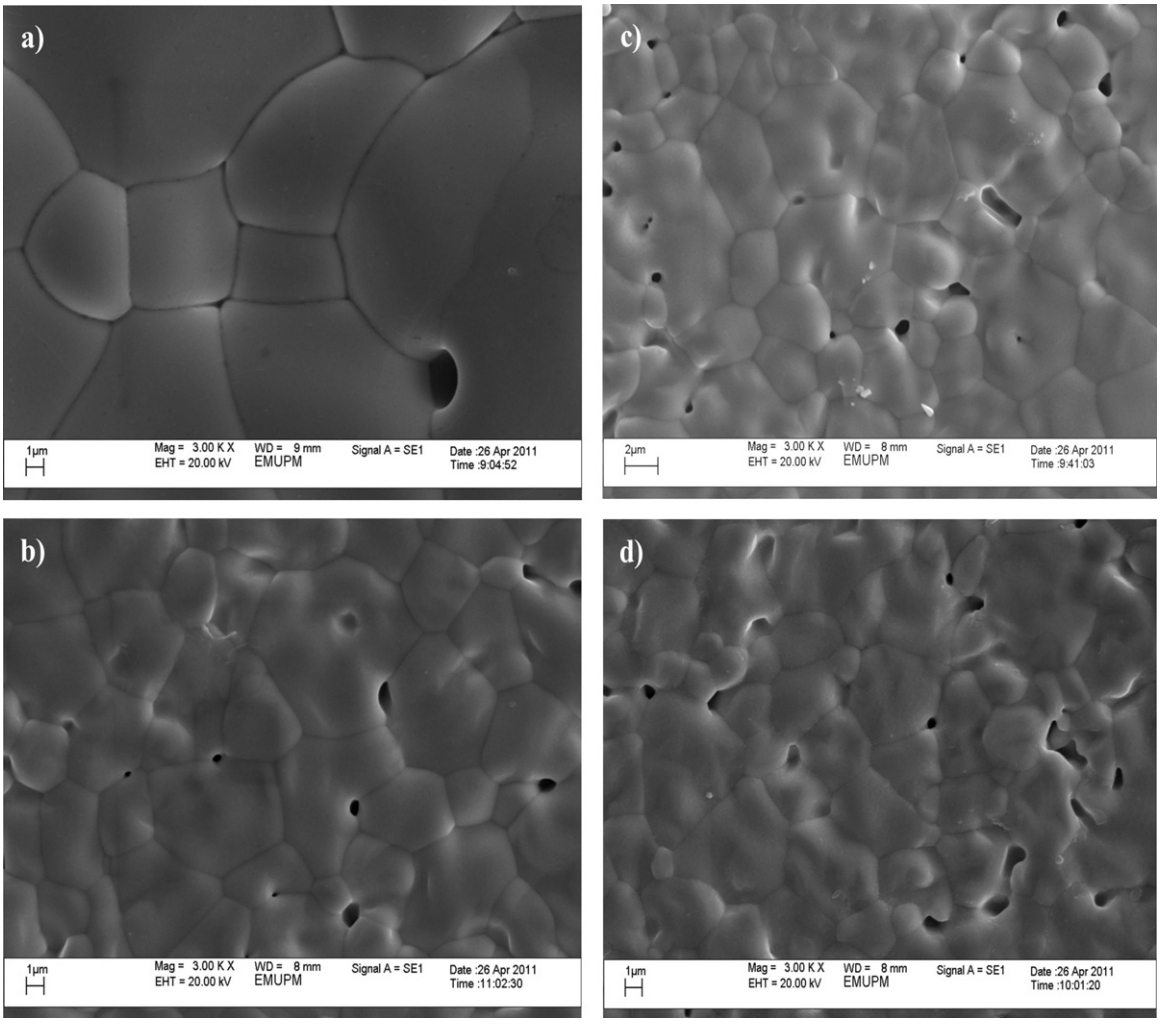

Fig. 8. SEM micrographs of BCT samples at 3 K magnification: (a) $x = 0$, (b) $x = 0.20$, (c) $x = 0.40$ and (d) $x = 0.60$.

BCT samples could be probably attributed to the removal of larger bismuth cation as mentioned earlier. On the other hand, the growth rate of grain size is also governed by diffusion mechanism within the sample in which oxygen content appears as one of the predominant factors. Annealing conditions such as prolonged heating duration or increased temperature could result in different diffusion rates of ionic species which affect the grain growth rate [30,31].

3.3. Structural Characterisation

The FTIR analysis is carried out in the absorption range of 1000–250 cm^{-1} and the spectra are shown in Fig. 9. The region of interest in this study is below 1000 cm^{-1} as the vibrations of the ions in the pyrochlore are normally not observed above 1000 cm^{-1} [32]. The pyrochlore oxides with different cations in either A or B site may appear as distinct configurations because the exact positions of atoms might change slightly [33]. The absorption bands at about 300 cm^{-1} [7] and 400 cm^{-1} are featured as A–O stretching vibration modes in the AO_6O_2' polyhedron. The absorption bands at approximately 650–520 cm^{-1} can be assigned to B–O stretching mode where it is

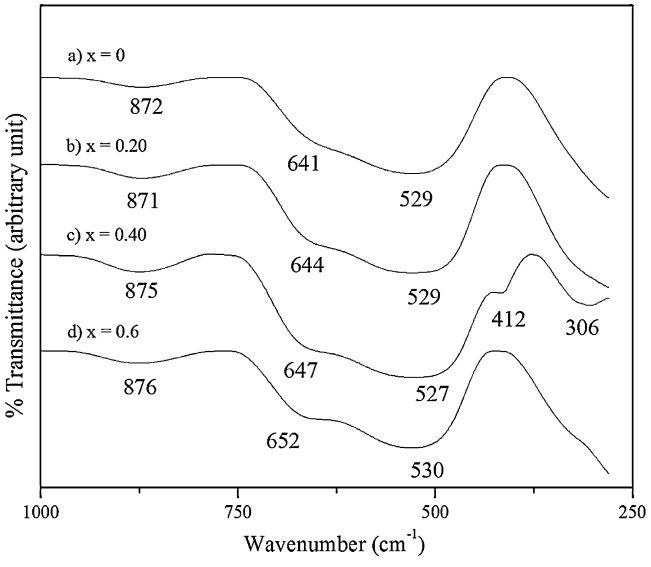

Fig. 9. IR spectra of BCT with constant mole % of copper.

Table 2
Peak position and types of the corresponding vibrational modes (cm^{-1}) in $Bi_{3-x}Cu_{1.8}Ta_{3+x}O_{13.8+x}$ pyrochlores.

Assignment	$x = 0$	$x = 0.2$	$x = 0.4$	$x = 0.6$
υ(A–O)	[a]	[a]	306, 412	[a]
υ(Ta–O–Ta)	872	871	875	876
υ(Ta–O)	529, 641	529, 644	527, 647	520, 652

[a] No peak is observed.

attributed to Ta–O [34,35]. Two broad absorption bands are observed at this range, particularly for the sample with higher tantalum content, $x = 0.6$ where the peaks are well resolved and can be distinguished clearly from the samples with lower Ta content. Furthermore, with an increase of Ta concentration, it is noticed that the absorption bands (~640–650 cm^{-1}) of Ta–O are slightly shift to higher frequencies. The absorption band at ~870 cm^{-1} is featured as Ta–O–Ta stretching mode [35] and all the FTIR results are summarised in Table 2.

3.4. Electrical properties

Fig. 10 represents the Arrhenius conductivity plots of phase pure BCT samples and their activation energies are relatively low for which the values fall in between 0.34 eV and 0.42 eV; a change in composition does not seem to result in different conductivities as similar and overlapped straight lines are observed. The total conductivity values, Y' extracted at room temperature are in the order of 10^{-7}–10^{-6} and the conductivities of BCT samples are of temperature dependent as these materials become more conductive at higher temperature arising from an increase numbers of thermally activated charge carriers (Fig. 11). In general, there are two discernable semicircles in BCT samples as shown in Cole–Cole plot of composition, $x = 0.2$ (Fig. 12). These semicircles can be

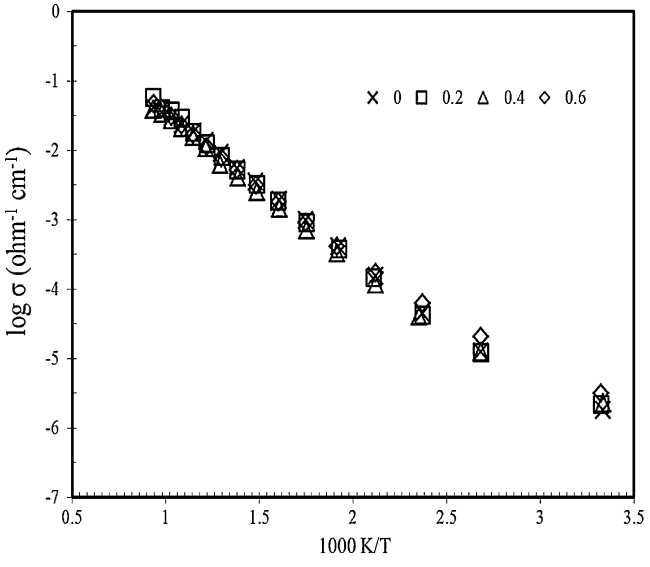

Fig. 10. Arrhenius conductivity plot of $Bi_{3-x}Cu_{1.8}Ta_{3+x}O_{13.8+x}$, for $0 \leq x \leq 0.6$.

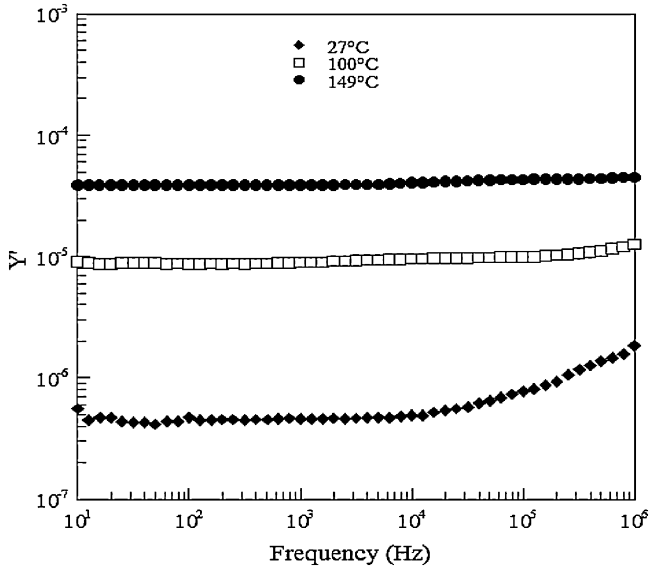

Fig. 11. Real part of admittance, Y' as a function of frequency for $Bi_3Cu_{1.8}Ta_3O_{13.8}$.

observed at ~28 °C and then vanished as the temperature increases. The inset figure illustrates an incomplete arc for composition, $x = 0.2$ which measured at temperature above 100 °C. The imaginary part of impedance, Z'' as a function of frequency on a logarithmic scale for composition $x = 0.2$ is shown in Fig. 13. The maximum of the curves decrease with increase of temperatures and they are displaced towards higher frequency region as the temperature increases. The existence of two peaks indicates that the polarisation processes have been taken place [36]. The modulus spectroscopic plot (Fig. 14) implies that the sample is electrically non-homogeneous as there are two observable maxima exist in imaginary part of Z''. The full width at half maximum (FWHM) of the M'' is ~1.36 decade which deviates from 1.14 decades of an ideal Debye response.

Dielectric loss as a function of temperature and frequency for the monophasic pyrochlores are plotted and shown in

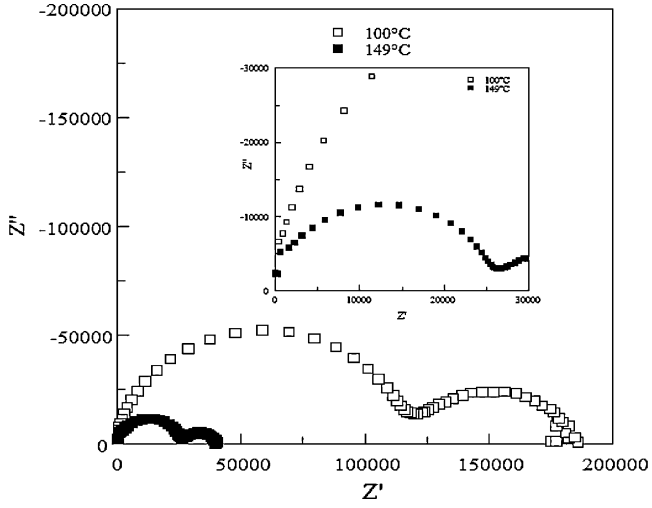

Fig. 12. Cole–cole plots of $Bi_{2.8}Cu_{1.8}Ta_{3.2}O_{14}$ measured at 100 °C and 149 °C.

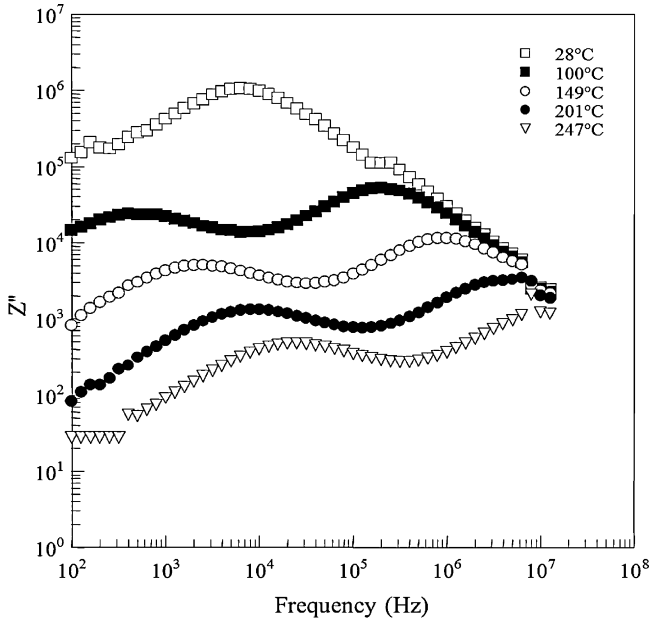

Fig. 13. Imaginary part of impedance, Z'' as a function of frequency for $x = 0.2$ measured at different temperatures.

Fig. 15a and b, respectively. Composition, $x = 0$ behaves predominantly insulating with electrical resistivity, $\rho = 2.2 \times 10^6\ \Omega$ cm and dielectric loss, tan δ, 0.06 at room temperature. High dielectric loss at low frequencies (Fig. 15b) might be attributed to time availability for the displacement of defects and energy is lost through the movement of the screen charge against the applied field [37]. In contrast to α-BZT analogue with low dielectric loss, increase of tan δ of Cu-based pyrochlore is possibly associated with the changes in valence state of the Cu ion and oxygen non-stoichiometry within the structure [6,9,38]. The oxidation and reduction processes involving oxygen and copper ions are presumably to be taken

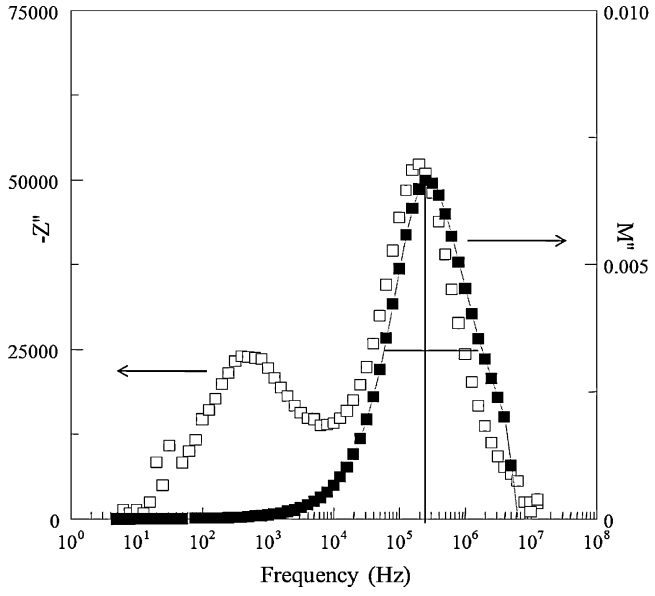

Fig. 14. Modulus spectroscopic plot of $Bi_{2.8}Cu_{1.8}Ta_{3.2}O_{14}$.

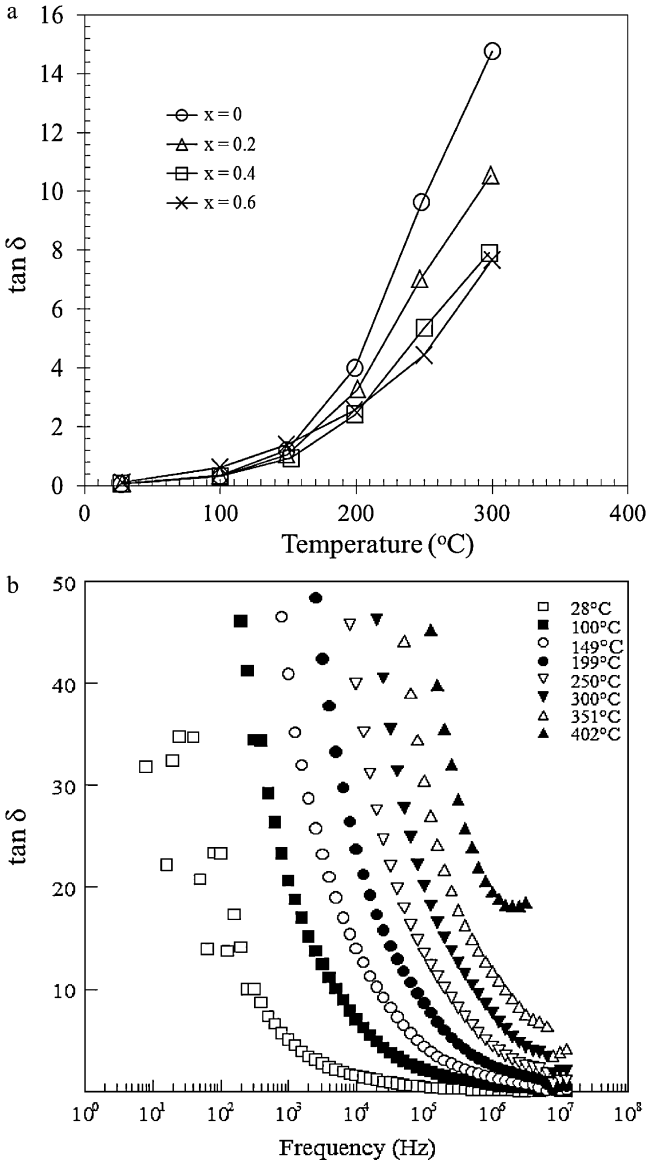

Fig. 15. (a) Dielectric loss as a function of temperature for samples $0 \le x \le 0.6$. (b) Tan δ as a function of frequency for $Bi_{2.4}Cu_{1.8}Ta_{3.6}O_{14.4}$.

place as suggested below:

$$2O^{2-} \leftrightarrow O_2 + 4e^- \quad (3)$$

$$Cu^{2+} + e^- \leftrightarrow Cu^+ \quad (4)$$

In our speculation, oxygen non-stoichiometry occurs appreciably at high temperature resulted from O^{2-} loss starting at temperature above 400 °C [39]. More vacancies and defects are created within the pyrochlore structure. With the release of electrons (Eq. (3)) Cu^{2+} will be reduced into Cu^+ that gives rise to the mixed conduction which associated with both ions and electrons. On the other hand, the cuprous ion, Cu^+ which is less stable in nature will be easily oxidised to cupric ion, Cu^{2+}. The hopping of oxygen ion had been suggested as the influential behavior of the conducting mechanism of pyrochlore oxides [31] and the higher defect concentrations and/or conductive behaviour of the samples could result in higher dielectric loss

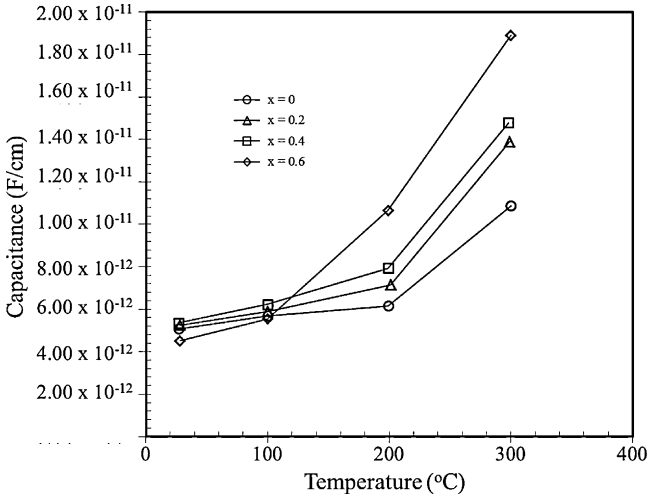

Fig. 16. Capacitance values of constant mole percent of BCT solid solution measured at 1 MHz.

Table 3
Electrical data for capacitance, relative permittivity, dielectric loss and admittance values for $Bi_{3-x}Cu_{1.8}Ta_{3+x}O_{13.8+x}$ pyrochlores measured at 1 MHz and room temperature.

	Capacitance, C_p (F cm^{-1})	Permittivity, ε'	Dielectric loss, tan δ	Admittance, Y' (Ω^{-1} cm^{-1})
$x = 0$	5.07×10^{-12}	57	0.06	1.86×10^{-6}
$x = 0.2$	5.25×10^{-12}	59	0.07	2.21×10^{-6}
$x = 0.4$	5.35×10^{-12}	60	0.07	2.33×10^{-6}
$x = 0.6$	4.51×10^{-12}	51	0.11	3.17×10^{-6}

[40]. This is clearly illustrated as tan δ increases with the increase of temperatures (Fig. 15a). Meanwhile, various papers have been reported on the mixed conduction behavior of Cu-based materials [41–43], however, actual conduction mechanisms are yet remained unclear. Given these discrepancies and uncertainties over the literature, thorough and careful investigations are certainly required before firm conclusions could be drawn in order to correlate the electrical–structural–compositional behavior of these BCT pyrochlore phases.

Fig. 16 shows the capacitance values of $Bi_{3-x}Cu_{1.8}Cu_{1.8}Ta_{3+x}O_{13.8+x}$ subsolidus solution measured at 1 MHz and these samples are of temperature dependent, showing positive temperature coefficient of capacitance, TCC values. The values of capacitance, ε', tan δ and Y' of BCT pyrochlores extracted from room temperature are tabulated in Table 3. Interestingly, BCT pyrochlores show comparable capacitance and ε' values to that of α-BZT analogues except their high dielectric losses due to high admittances as mentioned earlier.

4. Conclusion

A series of non-stoichiometric BCT sample had been successfully prepared and characterised. The $Bi_{3-x}Cu_{1.8}Cu_{1.8}Ta_{3+x}O_{13.8+x}$ subsolidus solution limit was determined as $0 \leq x \leq 0.6$ after heat treatment at 950 °C for 48 h. These materials were thermally stable within the studied temperature range. The internal strain values of BCT pyrochlores were generally low but slightly higher at both end-members. The crystallite sizes of prepared BCT pyrochlores estimated by Scherrer and Williamson–Hall methods were highly inter-correlated. The peaks situated at 650–520 cm^{-1} were featured to be Ta–O stretching mode and they were well separated for higher Ta concentration. The BCT system exhibited conductive characteristic at high temperature where tan δ became temperature dependent. The recorded activation energies for prepared samples were relatively low and the conduction mechanisms were likely influenced by variable oxidation state of copper ion and oxygen non-stoichiometry within the pyrochlore structure.

Acknowledgements

We thank the Ministry of Higher Education, Malaysia for financial support through Fundamental Research Grant and also the Ministry of Science, Technology, and Innovation Malaysia (MOSTI) for M.P. Chon's National Science Fellowship (NSF).

References

[1] Q. Wang, H. Wang, X. Yao, Structure, dielectric and optical properties of $Bi_{1.5+x}ZnNb_{1.5}O_{7+1.5x}$ pyrochlores, Ceram. Int. 35 (2009) 143–146.
[2] H. Du, X. Yao, Investigations on structural evolution and dielectric characteristics of high performance Bi-based dielectrics, Mater. Res. Bull. 40 (2005) 1527–1535.
[3] J.C. Nino, M.T. Lanagan, C.A. Randall, Dielectric relaxation in Bi_2O_3–ZnO–Nb_2O_5 cubic pyrochlores, J. Appl. Phys. 89 (2001) 4512–4516.
[4] H. Du, X. Yao, Structural trends and dielectric properties of Bi-based pyrochlores, J. Mater. Sci. Mater. Electron. 15 (2004) 613–616.
[5] A. Mergen, H. Zorlu, M. Özdemir, M. Yumak, Dielectric properties of Sm, Nd and Fe doped $Bi_{1.5}Zn_{0.92}Nb_{1.5}O_{6.92}$ pyrochlores, Ceram. Int. 37 (2011) 37–42.
[6] T.A. Vanderah, T. Siegrist, M.W. Lufaso, M.C. Yeager, R.S. Roth, J.C. Nino, S. Yates, Phase formation and properties in the system Bi_2O_3:2-CoO_{1+x}:Nb_2O_5, Eur. J. Inorg. Chem. 2006 (2006) 4908–4914.
[7] M. Chen, D.B. Tanner, J.C. Nino, Infrared study of the phonon modes in bismuth pyrochlores, Phys. Rev. B: Condens. Matter Mater. Phys. 72 (2005), 054303–1–8.
[8] Y. Liu, R.L. Withers, H. Chen, Q. Li, H. Tan, Raman spectra, photoluminescence and dielectric relaxation in $Bi_{1.5}ZnNb_{1.5}O_7$ pyrochlore, Curr. Appl. Phys. 11 (2011) S171–S174.
[9] D.P. Cann, C.A. Randall, T.R. Shrout, Investigation of the dielectric properties of bismuth pyrochlores, Solid State Commun. 100 (1996) 529–534.
[10] M. Valant, D. Suvorov, Chemical compatibility between silver electrodes and low-firing binary-oxide compounds: conceptual study, J. Am. Ceram. Soc. 83 (2000) 2721–2729.
[11] M.A. Subramanian, G. Aravamudan, G.V. Subba Rao, Oxide pyrochlores – a review, Prog. Solid State Chem. 15 (1983) 55–143.
[12] J. Xu, E. Ito, D. Yamazaki, X. Guo, X. Wu, Synthesis and crystal chemical characterization of the pyrochlore type $MgZrSi_2O_7$, Mater. Chem. Phys. 128 (2011) 410–412.
[13] I. Levin, T.G. Amos, J.C. Nino, T.A. Vanderah, C.A. Randall, M.T. Lanagan, Structural study of an unusual cubic pyrochlore $Bi_{1.5}Zn_{0.92}Nb_{1.5}O_{6.92}$, J. Solid State Chem. 168 (2002) 69–75.
[14] H. Youn, T. Sogabe, C.A. Randall, T.R. Shrout, M.T. Lanagan, Phase relations and dielectric properties in the Bi_2O_3–ZnO–Ta_2O_5 system, J. Am. Ceram. Soc. 84 (2001) 2557–2562.
[15] A. Mergen, W.E. Lee, Crystal chemistry, thermal expansion and dielectric properties of $(Bi_{1.5}Zn_{0.5})(Sb_{1.5}Zn_{0.5})O_7$ pyrochlore, Mater. Res. Bull. 32 (1997) 175–189.

[16] C. Ang, Z. Yu, H.J. Youn, C.A. Randall, A.S. Bhalla, L.E. Cross, J. Nino, M. Lanagan, Low-temperature dielectric relaxation in the pyrochlore $(Bi_{3/4}Zn_{1/4})_2(Zn_{1/4}Ta_{3/4})_2O_7$ compound, Appl. Phys. Lett. 80 (2002) 4807–4809.
[17] H. Youn, C. Randall, A. Chen, T. Shrout, M.T. Lanagan, Dielectric relaxation and microwave dielectric properties of Bi_2O_3–ZnO–Ta_2O_5 ceramics, J. Mater. Res. 17 (2002) 1502–1506.
[18] C.C. Khaw, K.B. Tan, C.K. Lee, High temperature dielectric properties of cubic bismuth zinc tantalate, Ceram. Int. 35 (2009) 1473–1480.
[19] X. Wang, H. Wang, X. Yao, Structures, phase transformations, and dielectric properties of pyrochlores containing bismuth, J. Am. Cerm. Soc. 80 (10) (1997) 2745–2748.
[20] R.D. Shannon, Revised effective ionic radii and systematic studies of interatomic distances in halides and chalcogenides, Acta Crystallogr. A 32 (1976) 751.
[21] K.B. Tan, C.C. Khaw, C.K. Lee, Z. Zainal, G.C. Miles, Structure and solid solution mechanisms of pyrochlore phases in the systems Bi_2O_3–ZnO–$(Nb, Ta)_2O_5$, J. Alloys Compd. 508 (2010) 457–462.
[22] G.C. Miles, A.R. West, Pyrochlore phases in the system ZnO–Bi_2O_3–Sb_2O_5: II. Crystal structures of $Zn_2Bi_{3.08}Sb_{2.92}O_{14+\delta}$ and $Zn_{2+x}Bi_{2.96-(x-y)}Sb_{3.04-y}O_{14.04+\delta}$, Solid State Sci. 8 (2006) 1422–1429.
[23] L. Cai, A.L. Arias, J.C. Nino, The tolerance factors of the pyrochlore crystal structure, J. Mater. Chem. 21 (2011) 3611–3618.
[24] V.M. Goldschmidt, The laws of crystals chemistry, Naturwissenschaften 14 (1926) 477–485.
[25] D.Y. Suarez, I.M. Reaney, W.E. Lee, Relation between tolerance factor and T-c in Aurivillius compounds, J. Mater. Res. 16 (11) (2001) 3139–3149.
[26] R. Yogamalar, V. Mahendran, R. Srinivasan, A. Beitollahi, R.P. Kumar, A.C. Bose, A. Vinu, Gas-sensing properties of needle-shaped Ni-doped SnO_2 nanocrystals prepared by a simple sol–gel chemical precipitation method, Chem. Asian J. 5 (2010) 2379–2385.
[27] T. Ungar, Microstructural parameters from X-ray diffraction peak broadening, Scr. Mater. 51 (2004) 777–781.
[28] G.K. Williamson, W.H. Hall, X-ray line broadening from filed aluminium and wolfram, Acta Metall. 1 (1953) 22–31.
[29] R. Yogamalar, R. Srinivasan, A. Vinu, K. Ariga, A.C. Bose, X-ray peak broadening analysis in ZnO nanoparticles, Solid State Commun. 149 (2009) 1919–1923.
[30] M. Sellami, V. Caignaert, M. Hamdad, A. Bekka, N. Bettahar, Synthesis and characterization of new pyrochlore solid solution $Bi_{1.5}Sb_{1.5-}Cu_{1-x}Mn_xO_7$, J. Alloys Compd. 482 (2009) 13–18.
[31] P.J. Wilde, C.R.A. Catlow, Defects and diffusion in pyrochlore structured oxides, Solid State Ionics 112 (1998) 173–183.
[32] V.A.M. Brabers, Infrared spectra of cubic and tetragonal manganese ferrites, Phys. Status Solidi (b) 33 (1969) 563–572.
[33] B.J. Kennedy, Structural trends in pyrochlore-type oxides, Phys. B 303 (1998) 241–243.
[34] D. Huiling, Y. Xi, Evolution of structure and dielectric properties on bismuth-based pyrochlore with TiO_2 incorporation, J. Electroceram. 9 (2002) 117–124.
[35] J. Masse, H. Szymanowski, O. Zabeida, A. Amassian, J.E. Klemberg-Sapieha, L. Martinu, Stability and effect of annealing on the optical properties of plasma-deposited Ta_2O_5 and Nb_2O_5 films, Thin Solid Films 515 (2006) 1674–1682.
[36] M.A.L. Nobre, S. Lanfredi, The effect of temperature on the electric conductivity property of $Bi_3Zn_2Sb_3O_{14}$ pyrochlore type phase, J. Mater. Sci. Mater. Electron. 13 (2002) 235–238.
[37] J.M. Herbert, Ceramics Dielectric and Capacitors, Gordon and Breach Science Publishers, 1985.
[38] M.A.L. Nobre, S. Lanfredi, Dielectric properties of $Bi_3Zn_2Sb_3O_{14}$ ceramics at high temperature, Mater. Lett. 47 (2001) 362–366.
[39] A.R. West, Basic Solid State Chemistry, second ed., John Wiley & Sons, Ltd., 2003.
[40] Y. Hu, C. Huang, Structural characterization of Bi–Zn–Nb–O cubic pyrochlores, Ceram. Int. 30 (2004) 2241–2246.
[41] H. Nguyen Ngoc, F. Petitbon, P. Fabry, Investigations on the mixed conductivity of copper tantalate, Solid State Ionics 92 (1996) 183–192.
[42] A. Heerwig, R. Merkle, J. Maier, M. Ruck, $Cu_{22}Bi_{12}S_{21}Cl_{16}$ – a mixed conductor with fast one-dimensional copper(I) ion transport, J. Solid State Chem. 184 (2011) 191–198.
[43] Y. Shen, A. Joshi, M. Liu, K. Krist, Structure, microstructure and transport properties of mixed ionic–electronic conductors based on bismuth oxide Part I. Bi–Y–Cu–O system, Solid State Ionics 72 (1994) 209–217.